Invariant Manifolds near L_1 and L_2 in the Sun-Jupiter Elliptic Restricted Three-Body Problem II. The dynamics of comet Oterma*

Gladston Duarte[(1)] and Àngel Jorba[(2,3)]

September 19, 2023

(1) Dipartimento di Ingegneria Meccanica e Aerospaziale, Politecnico di Torino, Via Duca degli Abruzzi 24, 10129, Torino, Italy.

(2) Departament de Matemàtiques i Informàtica, Universitat de Barcelona, Gran Via de les Corts Catalanes 585, 08007 Barcelona, Spain.

(3) Centre de Recerca Matemàtica, Edifici C, Campus Bellaterra, 08193 Bellaterra, Spain

E-mails: <gladston.duarte@polito.it>, <angel@maia.ub.es>.

Abstract

Comet 39P/Oterma is known to make fast transitions between heliocentric orbits outside the orbit of Jupiter and heliocentric orbits inside that of Jupiter. In this paper, the dynamics of comet Oterma is modelled and fitted in the Planar Elliptic RTBP. Using the computations presented in [DJ23a] we look for the invariant objects around L_1 and L_2, which in the case of the Planar Elliptic RTBP are invariant tori and their stable and unstable manifolds, that are the skeleton that guides Oterma in its rapid transition.

Keywords : Planar Elliptic Restricted Three-Body Problem; Lagrangian points; Rapid transition mechanism; Comet 39P/Oterma.

*This work has been supported by the Spanish grant PID2021-125535NB-I00 (MCIU/AEI/FEDER, UE) and the catalan grant 2021 SGR 01072. G.D. acknowledges the support from the Spanish Ministry of Economy and Competitiveness through the "María de Maeztu" Programme for Units of Excellence in R&D (MDM-0445-2014) and the support of Polish National Science Centre grant 2018/29/B/ST1/00109.

Contents

1 Introduction

39P/Oterma is a comet orbiting the Sun, currently inactive, that has experienced fast transitions between orbits inside and outside that of Jupiter. This is illustrated in Figure 1 where some plots of the trajectory of Oterma are shown. Oterma is not the only comet that have this type of behaviour. Some other comets to have similar type of behaviour are 36P/Whipple, 82P/Gehrels, 129P/Shoemaker-Levy 3 and 147P/Kushida-Muramatsu ([OIY$^+$08]). Some of them experience a Rapid Transition Mechanism, some complete at least one full revolution around Jupiter, and some have collided.

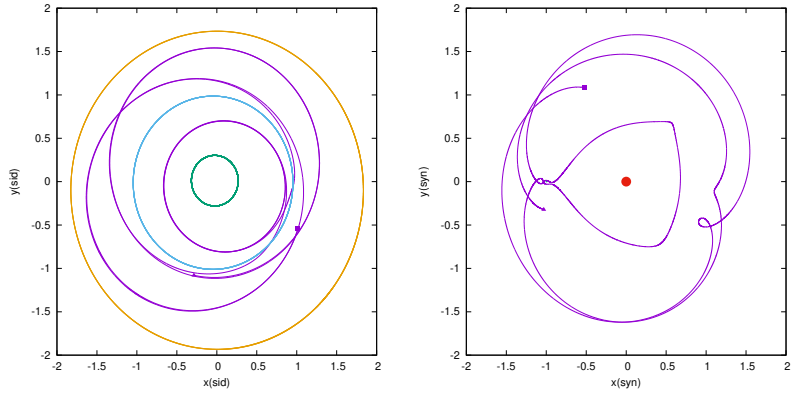

(a) (b)

Figure 1: Transition of Oterma. (a) Inertial frame and (b) Roto-pulsating frame. In both cases Oterma's orbit is shown in purple, the initial point (highlighted as a triangle) is January 1$^{\text{st}}$, 1900 and the final one (a square) is January 1$^{\text{st}}$, 2000. In (a) the orbits of Mars (green), Jupiter (blue) and Saturn (orange) are also shown, while in (b) just Jupiter (the blue dot near $(-1, 0)$) and the Sun (the red dot near $(0, 0)$) are shown. These graphs are obtained by integrating the whole Solar System and plotting some of the objects. The unit of distance is the Sun-Jupiter mean distance.

These transitions were first studied in [KLMR01], where the authors explain a mechanism that permits Oterma to experience the phenomenon of transition between different regions in the configuration space. Such mechanism is known as Rapid Transition Mechanism and it is characterized by a transition without completing a revolution around (in this case) Jupiter. It is important to note that these transitions are based on passages near the collinear points $L_{1,2}$ of the Sun-Jupiter system, and that the transitions are organised by the stable/unstable manifolds of the Lyapunov periodic orbits around these points. An explicit computation of the manifolds is done in [DJ23b] by means of normal form computations. It is remarkable that, for the Planar RTBP, these normal forms are convergent.

In this paper we plan to study this transition in more general models. We will first perform some numerical simulations with a realistic motion of Jupiter and including the effect of other planets, to see which perturbations have a relevant role in the transition. As we will see, the main effect to be included to the Planar RTBP to model more accurately the transition of Oterma is the eccentricity of Jupiter. This is not a surprise since a small change in the position of Jupiter has a big impact in the passages near $L_{1,2}$. These simulations suggest that the Planar Elliptic RTBP (PERTBP) is a very good model for the study of the transition. Therefore, this is model we have used here to study the motion of Oterma. Using the calculations of invariant tori and invariant manifolds from [DJ23a] we identify the 2D invariant tori near $L_{1,2}$ whose invariant manifolds guide

the transit of Oterma.

1.1 The Planar Elliptic Restricted Three-Body Problem

The PERTBP is a special configuration of the n-Body Problem, with $n = 3$: two of the bodies are massive (they are usually called primaries) while the third body has negligible mass (usually called secondary) so it does not affect the motion of the primaries but it is attracted by them. Therefore, the primaries move as in a two body problem. Here we assume that the two primaries move on an elliptic orbit of eccentricity e and that the secondary moves in the plane of of motion of the primaries. As usual, the goal of the problem is to describe the motion of the secondary.

A common reference frame is the synodical system of coordinates. It is defined with origin at the centre of mass of the primaries, and with axis that revolves with the same angular velocity as the primaries so that they are kept on the x axis for all times. Note that, as the motion of the primaries is not circular but elliptic, the rotation velocity is not constant. The unit of distance is chosen as the distance between the primaries. This means that this unit depends periodically on time. The y axis is perpendicular to the x axis (and inside the plane of motion). The orientation is that x, y and the angular momentum of the two primaries is positive definite. The unit of time is such that the period of the primaries is 2π and the unit of mass is such that the total mass of the primaries is 1. It is usual to call μ the mass of the smallest primary. In these coordinates, the primaries do not move, they stand still in two points: the one of mass μ in $(-1+\mu, 0, 0)$ and the one of mass $1-\mu$ in $(\mu, 0, 0)$.

As the solution of the two-body problem is easily described as as function of the true anomaly (it is also possible to use the eccentric anomaly) instead of a function of time (see [Pol66, Roy04]), it is usual to write the equations of motion not as a function of time but as function of one of these anomalies. Here we have chosen the true anomaly as it is explained in [Sze67]. It turns out that the equations of motion are Hamiltonian, with the following Hamilton function,

$$H(x, y, p_x, p_y, f) = \frac{1}{2}\left((p_x + y)^2 + (p_y - x)^2\right) - \frac{1}{1 + e\cos f}\left(\frac{1}{2}(x^2 + y^2) + \frac{1-\mu}{r_1} + \frac{\mu}{r_2}\right), \qquad (1)$$

where $r_1^2 = (x-\mu)^2 + y^2$ is the square of the distance of the secondary to the primary of mass $1-\mu$, $r_2^2 = (x+1-\mu)^2 + y^2$ is the square of the distance to the primary of mass μ, e is the eccentricity of the primaries and f is their true anomaly. Note that the independent variable is not the time but the true anomaly f.

This model is a two degrees of freedom Hamiltonian system that depends on "time" (i.e., the true anomaly f) in a 2π-periodic way. This implies that the Hamiltonian is not a first integral of the motion, so the phase space is, in fact, five-dimensional. Note that setting $e = 0$ the Hamiltonian for the circular RTBP is recovered and f becomes the time. Finally, for small values of e, the elliptic model can be seen as a 2π-periodic "time dependent" perturbation of the circular RTBP.

It is well-known that the equilibrium points of Hamiltonian (1) coincide with the equilibrium points of the circular RTBP [Sze67]. Therefore, there are 5 equilibrium points, three of them ($L_{1,2,3}$) are located on the x-axis: L_2 to the left of the primary located at $(-1+\mu, 0, 0)$, L_1 is between the primaries, and L_3 to the right of the primary located at $(\mu, 0, 0)$. There are two more points ($L_{4,5}$) located at the third vertex of an equilateral triangle where the other two vertices are the primaries.

Here we focus on the dynamics around the collinear points $L_{1,2}$. When $e = 0$ (that is, for the circular RTBP) is well known that these points are of centre×saddle type. In this case, the Lyapunov centre theorem ensures the existence of a one-parametric family of periodic orbits (usually called Lyapunov orbits) that can be seen as the continuation of the linear oscillations of the centre

directions to the nonlinear system [MO17]. When $e > 0$ but small, the effect of the periodic forcing given by the "time" f is that there exists a Cantor set of periodic orbits in this family that are not destroyed by the perturbation but they become quasi-periodic orbits with two basic invariant frequencies: the forcing frequency (1 in this case) plus the one of the periodic orbit they come from [JV97b]. Moreover, these quasi-periodic solutions are hyperbolic having stable and unstable manifolds, that come from the stable/unstable manifolds of the Lyapunov periodic orbits that exist when $e = 0$. These families of quasi-periodic orbits and their invariant manifolds have already been computed, for the Sun-Jupiter case, in [DJ23a].

1.2 Contributions

The first part of the paper (Section 2) is devoted to a numerical study of the motion of Oterma with different models of Solar system. The models are based on a classical n-body problem with the goal of finding the simplest model with a realistic transition of Oterma. In these simulations it is shown that the circular RTBP does not describe accurately the transitions of Oterma while the planar elliptic RTBP gives a trajectory which is similar to the one given by simulations including all the planets.

The second part of the paper (Section 4) uses the results from [DJ23a] to analyse this transition. In particular, we compute the invariant tori and invariant manifolds that are responsible for this transition, showing graphically how the motion of Oterma follows them in phase space.

This paper is structured as follows: Section 2 presents numerical experiments of the motion of Oterma using several models of Solar system, Section 3 explains how to compute the change of variables to translate Oterma from the real system to the PERTBP, and Section 4 shows how to visualize Oterma in the phase space of the PERTBP and how it relates with the computed objects (tori around L_1 and L_2 and their stable/unstable manifolds).

2 Numerical Experiments

In this Section we present some simulations of the motion of Oterma including the gravitational effect of the major bodies of the Solar system. The goal of this Section is to justify a better choice of the model to improve the description of Oterma's rapid transition. As usual, we look for the simplest model that contains a realistic description of the motion of the comet.

2.1 The motion of Oterma in the Solar system

The model used for a realistic simulation of the motion of Oterma is a Restricted $(N + 1)$-Body system, where Sun and planets are point masses and Oterma is an infinitesimal particle. The numerical integrator is a Taylor method ([JZ05]) with initial data for Sun, planets and Oterma extracted, in ecliptical coordinates, from the JPL Horizons system.

Figure 2, left, shows the distance (in AU) from Oterma to the Sun with respect to time in days (purple curve) during the 20th century. The distance from Mars (green), Jupiter (blue) and Saturn (orange) to the Sun is added for reference. Figure 2, right, displays the instantaneous semi-major axis of these bodies with respect to the Sun. There are two gaps in the semi-major axis of Oterma because, during the transitions, it passes very close to Jupiter so that its orbit is not close to a Keplerian orbit around the Sun and it makes no sense to compute its semi-major axis with respect to our star. These two gaps correspond to the periods that go from March 27tn 1936 until May 31st 1939, and from January 23rd 1963 until May 2nd 1964. This Figure 2 is an indicator of the

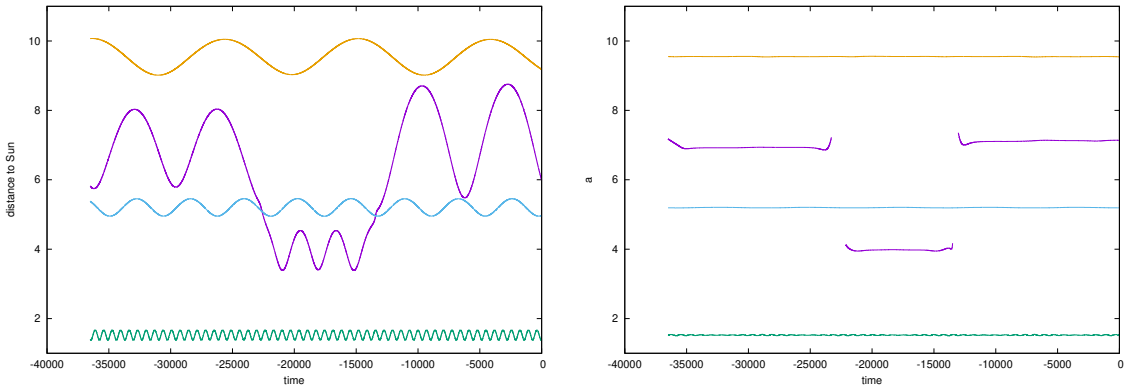

(a) (b)

Figure 2: Illustration of Oterma's transition using (a) distances from Mars (green), Jupiter (blue), Saturn (orange) and Oterma (purple), to the Sun, and (b) the semi-major axis of the same objects. Time spans from January 1st, 1900 until January 1st, 2000. The semi-major axis of Oterma is not computed in the transition regions since the approximation of its orbit by a Keplerian one is not valid. Time is given in days and distance in AU.

transition mechanism. This information can also be complemented by computing the distances between Oterma and Jupiter, to confirm that these fast transitions coincide with close approaches between these bodies. This is shown in Figure 3.

2.2 Reduced $(N+1)$-Body models

The goal of this section is to discuss models with less planets such that Oterma presents a transition similar to the one we have seen in the previous section. To this end, we have considered different sets of planets, and we only present the best results that correspond to the Sun-Jupiter-Oterma and Sun-Jupiter-Saturn-Oterma cases. The other cases produce a very similar transition and the effect of the extra planets on Oterma is only seen in much longer time spans. The simulations have been carried out by means of a high order Taylor method [JZ05].

An important point in these simulations is the choice of the time for the initial conditions of the involved bodies. The reason is that the initial conditions are taken when Oterma is approaching the transition (i.e., Jupiter) then the gravitational effect of Jupiter dominates the motion of the comet and effect of the other bodies becomes relatively small (this is also discussed in [DJ23b]). To help in the comparisons we will compute, at each integration time step, the semi-major axis of the osculating orbit of each body (planets and Oterma).

We start by considering the effect of only Sun and Jupiter on Oterma. This means that we obtain the initial data for Sun, Jupiter and Oterma from the JPL ephemeris. Assuming that the mass of Oterma is so small that it does not affect the motion of Sun and Jupiter, the motion of these two bodies follows Kepler's laws so that they move on ellipses, while Oterma is attracted by them. This model is usually known as Elliptic Restricted Three-Body Problem, ERTBP (see [Sze67]). We note that the motion of Oterma is not in the plane of motion of Sun and Jupiter so this is a 3D model.

Figure 4 shows the computed semi-major axis of Jupiter (which is constant in this model, it has only been added as a reference) and Oterma, for four different initial times. Note that, as the initial position of the bodies for two different times is related by their motion in the real Solar system, the

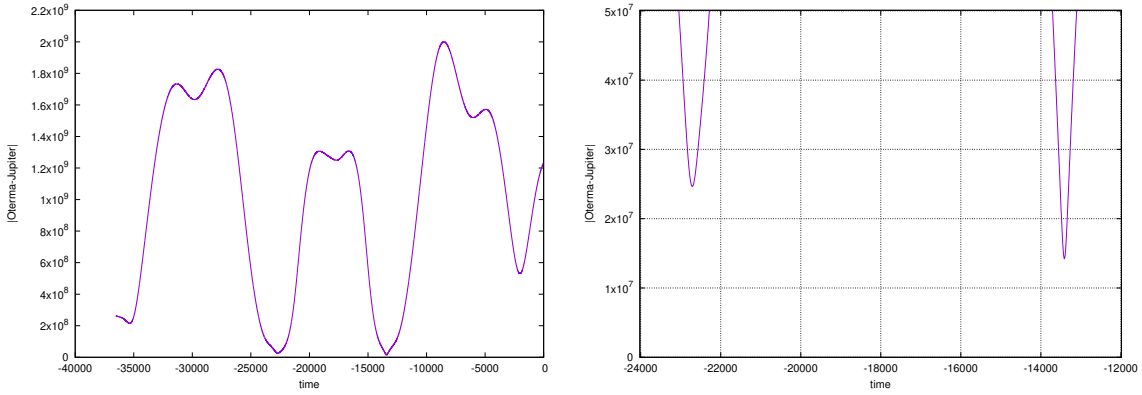

(a) (b)

Figure 3: Distance between Oterma and Jupiter during the 20th century. The units are km and days. (a) Complete time span; (b) Zoom in two regions where they approach.

corresponding orbits for Oterma in the ERTBP will be different. For this reason, the jumps in the semiaxis of Oterma in Figure 4 are not identical. It is important to note that the trajectory after a passage near Jupiter is quite sensitive to initial conditions and perturbations, so the differences in the jumps when changing the date of initial conditions for the ERTBP are expected. Moreover, as we take as the time of the initial data closer to the time where the transition occurs, the effect of the other planets become negligible.

2.3 Simplifying Sun-Jupiter-Oterma

Based on [KLMR01, DJ23b], the PCRTBP is enough for the Rapid Transition Mechanism to exist. Both Jupiter's eccentricity and the angle which Oterma interesects the Sun-Jupiter plane of movement are small ($e \approx 0.048594036027482114$ and $\alpha \approx 2.48603789613$ degrees, respectively), which justify these assumptions. However, when dealing with real data, it may be possible that this model is not enough.

There are some works done based in this behaviour that use the PCRTBP as a base model to analyse this dynamics (see, for instance, [KLMR01]) and, although $H = 3.03$ (the value of the Hamiltonian used by may authors) is a possible one for Oterma, there is no clear reason for choosing this specific value and not another.

We are aware of some works in the SCRTBP ([AEL17, GL18]), but not in the PERTBP.

Let us see that the PERTBP maintains (at least partially) the qualitative behaviour of Oterma.

In principle, it would be possible to project Oterma's position and velocity in many ways in the Sun-Jupiter's plane of movement, so the adopted strategy was choosing a time where Oterma was close to Jupiter (such chosen time is $t = -23500$ (August 30^{th}, 1935)) and orthogonally project Oterma's both position and velocity in the desired plane.

Figure 5 shows the distances from Jupiter and this projection of Oterma to the Sun, together with the semi-major axis of their osculating orbit, whenever this approxiamtion can be done, from August 30^{th}, 1935 until January 1^{st}, 2000, numerically integrated with a Taylor method.

It should be mentioned that, although the transition happens in the case of orthogonally projecting Oterma, analysing the Figure 5 one may consider, inspired by the time that the approximation by a Keplerian orbit cannot be done that Oterma does not experience a Rapid Transition Mechanism, and revolves around Jupiter. In order to check if this is the case, consider Figure 6.

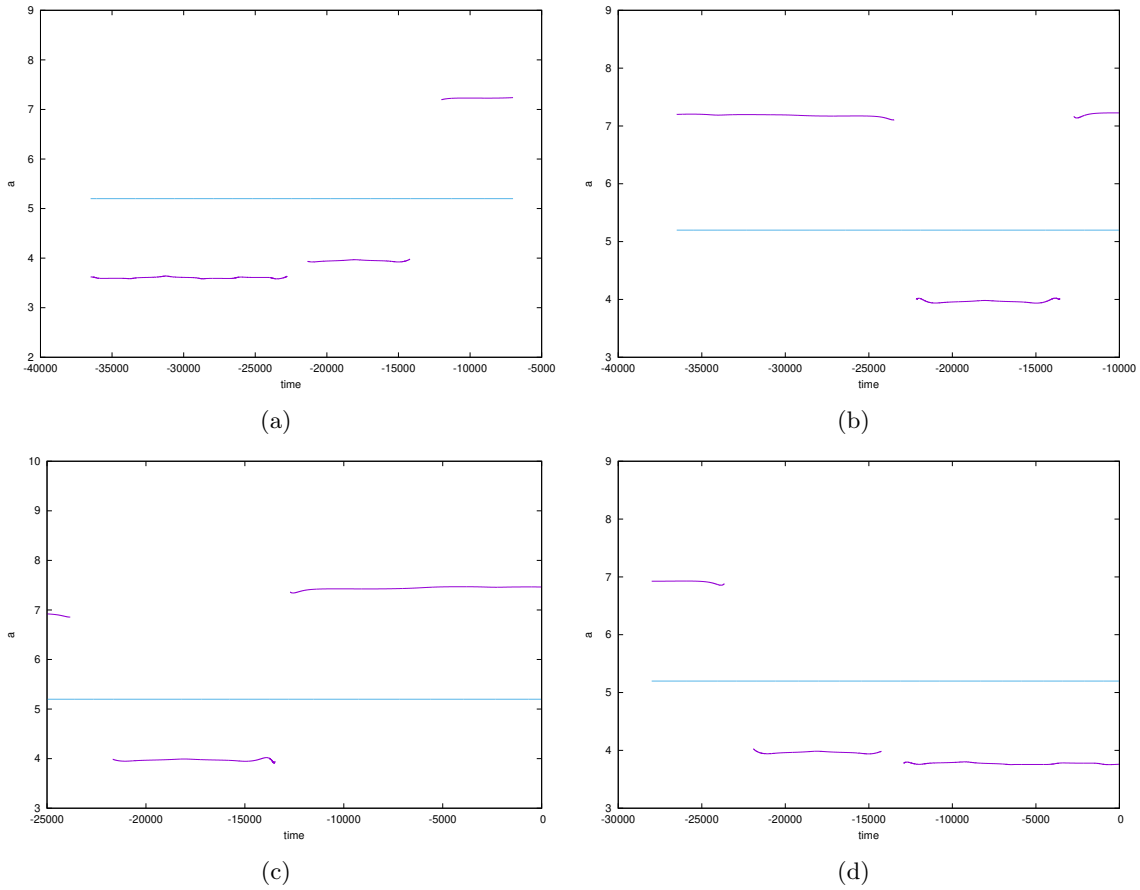

Figure 4: Semi-major axis of Jupiter (blue) and Oterma (purple) in the Elliptic RTBP. Units in AU and days. (a) Backward integration starting at $t = -7000$ (November 1^{st}, 1980); (b) Backward integration starting at $t = -10000$ (August 15^{th}, 1972); (c) Forward integration starting at $t = -25000$ (July 22^{nd}, 1931); (d) Forward integration starting at $t = -28000$ (May 5^{th}, 1923). Time is given in days and distance in AU.

Comparing Figures 6 and 1 we may see that Oterma's behaviour is affected by the chosen projection, and comparing Figures 6 and 7 we can conclude that, in fact, this change is a revolution around Jupiter so Oterma does not experience a Rapid Transition Mechanism, in the case of this projection. We do, however, use this set of initial data, in this specific initial time and this projection for all the analyses we make in this paper.

Notice that it also makes more sense to consider the eccentricity instead of the third dimension, because, at a given time, when considering the interaction between Sun and Jupiter, it is an elliptic orbit, so it is not needed to adjust their orbits, just Oterma's, while, when modelling this problem as a SCRTBP, we would have to use Jupiter's oscullating orbit, instead of the orbit itself.

We are aware that this represents an approximation to Oterma's orbit, although it is, by itself, a rich dynamics which a lot could be worked on and it may serve as one step more in the direction of understanding and modelling Oterma's behaviour.

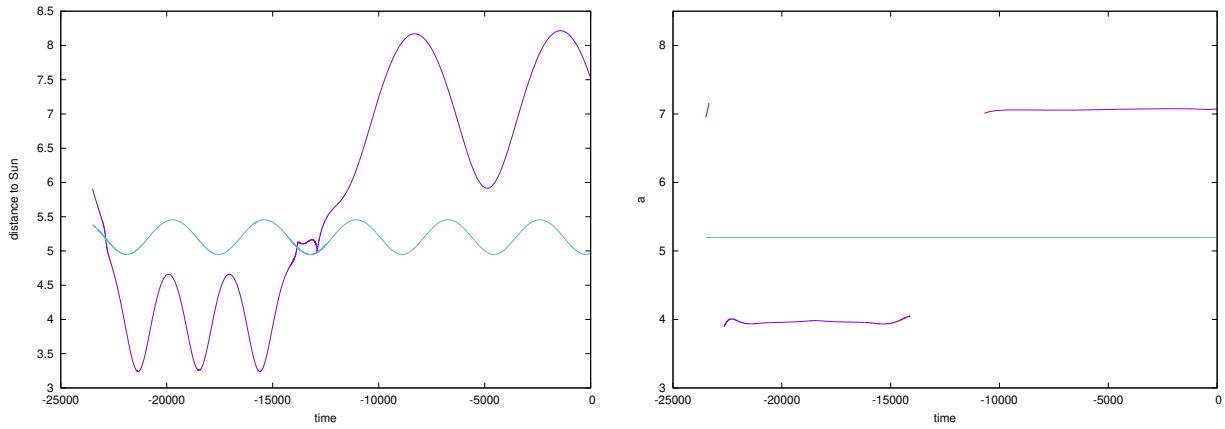

(a) (b)

Figure 5: (a) Distances from orthogonally projected Oterma and Jupiter to the Sun and (b) orthogonally projected Oterma's computed semi-major axis, with initial data in $t = -23500$ (August 30^{th}, 1935). Time is given in days and distance in AU.

3 Going from ecliptic to synodical ERTBP coordinates

As it has been mentioned above, the initial data for the bodies is taken from the JPL Horizons system in ecliptic coordinates (we also refer to these coordinates as sidereal). In this section we discuss how we transfer this initial data in sidereal coordinates to the synodical reference system of the ERTBP model (see also [GLMS01, JN20]).

Let $\vec{e}$, $\vec{a}$ be the position vectors of the comet in sidereal and in synodical coordinates, respectively. The arrow above e and a is to distinguish between the position vectors and the eccentricity and semi-major axis quantities. If the origin of coordinates is at the Sun-Jupiter barycentre, the change of coordinates is of the form

$$\vec{e} = KC\vec{a},$$

where $K = K(t)$ is a scalar and $C = C(t) \in \mathcal{M}_{3\times 3}(\mathbb{R})$ is an orthogonal matrix, both depending periodically on time (with the period of Jupiter). We need to compute the functions K and C.

Let us name $\vec{r}_S$, $\vec{r}_J$, $\vec{v}_S$, $\vec{v}_J$, $\vec{a}_S$, $\vec{a}_J$ as the position, velocity and acceleration vectors of the Sun and Jupiter in sidereal coordinates. Then, $K = \|\vec{r}_J - \vec{r}_S\|$ and $C = (C_0 \;\; C_1 \;\; C_2)$, where

$$C_0 = \frac{\vec{r}_J - \vec{r}_S}{\|\vec{r}_J - \vec{r}_S\|}, \quad C_2 = \frac{(\vec{r}_J - \vec{r}_S) \times (\vec{v}_J - \vec{v}_S)}{\|(\vec{r}_J - \vec{r}_S) \times (\vec{v}_J - \vec{v}_S)\|}, \quad C_1 = C_2 \times C_0.$$

Let us define $\vec{r} = \vec{r}_J - \vec{r}_S$, $\vec{v} = \vec{v}_J - \vec{v}_S$ and $\vec{a} = \vec{a}_J - \vec{a}_S$. With the above notation, and using a dot to denote the derivative with respect to time, we have that $\dot{K} = \dfrac{\vec{r}\cdot\vec{v}}{K}$ and $\dot{C} = (\dot{C}_0 \;\; \dot{C}_1 \;\; \dot{C}_2)$, with

$$\dot{C}_0 = \frac{-\vec{v}K + \dot{K}\vec{r}}{K^2}, \qquad \dot{C}_2 = \frac{\|\vec{w}\|\vec{u} - \dot{\vec{w}}\vec{w}}{\|\vec{w}\|^2}$$

and

$$\begin{aligned}\dot{C}_1 \quad = \quad & (C_{31}\dot{C}_{23} - C_{21}\dot{C}_{33} + C_{23}\dot{C}_{31} - C_{33}\dot{C}_{21} \\ & C_{11}\dot{C}_{33} - C_{31}\dot{C}_{13} + C_{33}\dot{C}_{11} - C_{13}\dot{C}_{31} \\ & C_{21}\dot{C}_{13} - C_{11}\dot{C}_{23} + C_{13}\dot{C}_{21} - C_{23}\dot{C}_{11}),\end{aligned}$$

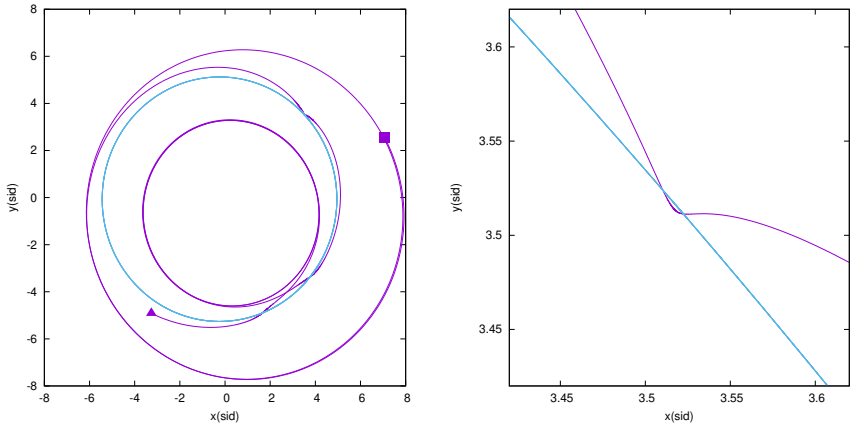

(a)

(b)

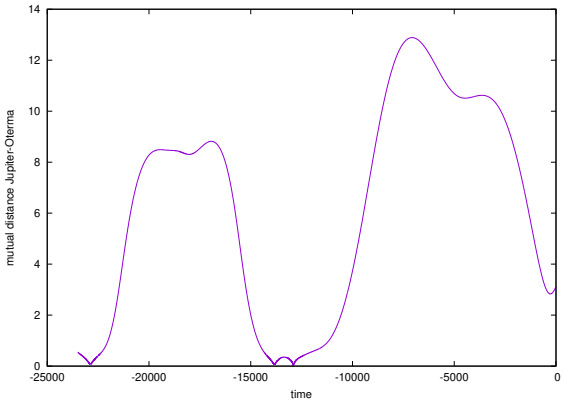

(c)

Figure 6: (a,b) Computed orbits of Jupiter (in green) and orthogonally projected Oterma (in purple), with initial data gathered in $t = -23500$ (August 30^{th}, 1935). (c) Mutual distance Oterma-Jupiter. Time is given in days and distance in AU.

where we have used that $\vec{w} = \vec{r} \times \vec{v}$, $\vec{u} = \vec{r} \times \vec{a}$, $\dot{\vec{w}} = \dfrac{\vec{w}\,\vec{u}}{\|\vec{w}\|}$. Now we can write

$$\dot{\vec{e}} = \dot{K}C\vec{a} + K\dot{C}\vec{a} + KC\dot{\vec{a}},$$

which is equivalent to

$$\dot{\vec{a}} = \frac{C^{-1}}{K}\left(\dot{\vec{e}} - \dot{K}C\vec{a} - K\dot{C}\vec{a}\right).$$

Using the chain rule, $\dfrac{d}{dt} = \dfrac{df}{dt}\dfrac{d}{df}$, we have that

$$\vec{a}\,' = \left(\frac{df}{dt}\right)^{-1}\frac{C^{-1}}{K}\left(\dot{\vec{e}} - \dot{K}C\vec{a} - K\dot{C}\vec{a}\right),$$

where $' = \dfrac{d}{df}$ and $\dfrac{df}{dt} = \dfrac{nl^{3/2}}{a^{3/2}(1-e^2)^{3/2}}(1 + e\cos f)^2$, being n the mean motion and l the mutual distance between the primaries. The values of f, n and l can be computed using the initial position and velocity data from the Sun and Jupiter, see for instance [VM01].

x	-3.269606195127012$\times 10^{0}$
y	-4.912907103387245$\times 10^{0}$
z	-1.062586015761811$\times 10^{-1}$
p_x	6.851123034929325$\times 10^{-3}$
p_y	-3.280793687151255$\times 10^{-3}$
p_z	-3.088020478441808$\times 10^{-4}$

Table 1: Oterma's coordinates at August 30$^{\text{th}}$ 1935 in the sidereal frame.

x	-1.0952439413131636$\times 10^{0}$
y	2.9918455882452549$\times 10^{-2}$
p_x	8.0698975794308611$\times 10^{-2}$
p_y	-1.0358302646539692$\times 10^{0}$
f	3.8817002439241626$\times 10^{0}$

Table 2: Oterma's coordinates at August 30$^{\text{th}}$ 1935 in the synodical roto-pulsating frame.

Therefore, the change of variables in positions and velocities is given by

$$\begin{cases} \vec{a} &= \dfrac{C^{-1}}{K}\vec{e}, \\ \vec{a}\,' &= \left(\dfrac{df}{dt}\right)^{-1} \dfrac{C^{-1}}{K}\left(\dot{\vec{e}} - \dot{K}C\vec{a} - K\dot{C}\vec{a}\right). \end{cases} \tag{2}$$

Collecting Oterma's position and velocities from the JPL Horizons system on August 30$^{\text{th}}$ 1935 (see Table 1) and applying (2) we obtain its positions and velocities in the synodical frame, shown in Table 2, where, as in [DJ23b], the coordinates have been orthogonally projected on the Sun-Jupiter plane. Integrating these initial conditions in the PERTBP equations, we have the orbit shown in Figure 7. Figure 7(b) shows a very close approach of Oterma with Jupiter but this is due to the scale of the plot (the radius of planet Jupiter is close to 71000 km while the minimum distance between Jupiter and Oterma, during these computations, is of 310969 km).

4 Oterma in the Planar Elliptic Restricted Three-Body Problem

In this section we discuss the computation of the dynamical objects responsible for Oterma's trnasition in the Planar Elliptic Restricted Three-Body Problem. The details of these computations are described in [DJ23a]. Therefore, here we focus on the visualisation and analysis of the role played by these dynamical objects in the transition of Oterma. As expected, these objects are given by the heteroclinic connections between invariant tori around the points L_1 and L_2 of the Elliptic problem.

Let us note that there is a fundamental difference between the circular and the elliptic models: while in the former, once a value for the Hamiltonian is chosen, the orbit gets confined in a three-dimensional submanifold of the four-dimensional phase space, this does not happen in the latter one: as the Hamiltonian function is not a first integral (since it depends on time) an orbit is not restricted to an energy level so the dynamics takes place in a truly five-dimensional phase space.

This difference leads to fundamental unalike roles of the manifolds of the invariant tori around L_1 and L_2. For the circular case, given a suitable energy level h_0, the Lyapunov periodic orbit

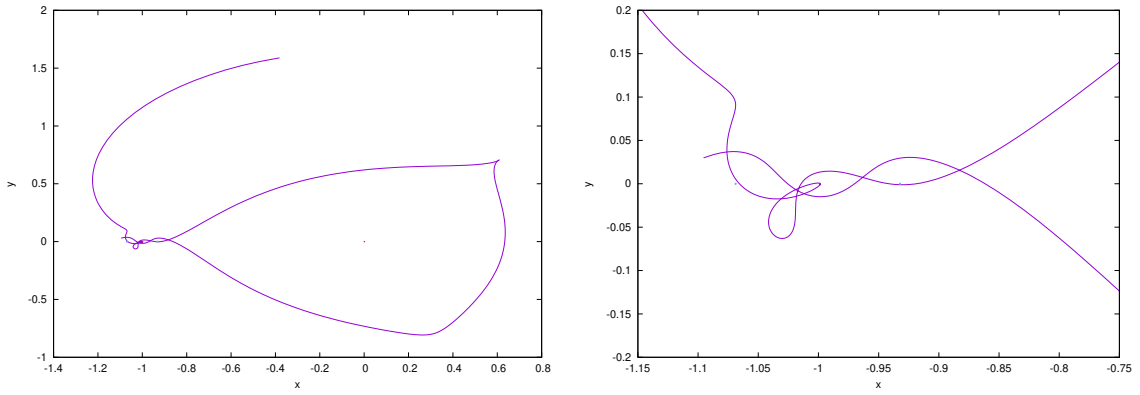

(a) (b)

Figure 7: Orthogonally projected Oterma's orbit integrated using the PERTBP equations of motion (in purple); in red, Jupiter and Sun (out of scale); and in blue, L_1 and L_2 positions. (b) Zoom in the region near Jupiter.

around L_1 and the one around L_2 in this energy level have dimension 1 and their stable and unstable manifolds have dimension 2. Hence, as their codimension inside the energy manifold $H = h_0$ is 1, they divide the region of possible motion in two. This is not what happens in the elliptic case, where the tori around L_1 and the ones around L_2 have dimension 2, their stable and unstable manifolds, dimension 3, so their codimension is 2, and they do not divide the regions of possible motion in two. This implies what is described in Section 3.7 of [KLMR01] about the stable and unstable manifolds of the periodic orbits being the separatrices between different types of orbit (transit and nontransit) is not true in the PERTBP, as it is not possible to define what is the inside and the outside of the manifolds.

The visualisation of these objects is not a trivial task. To reduce dimensionality, we can use the stroboscopic map given by the period of Jupiter so that the invariant tori near $L_{1,2}$ are invariant curves, and their stable/unstable manifolds are two dimensional, all of them inside a four-dimensional phase space. Moreover, note that the trajectory of Oterma in the stroboscopic map is a sequence of points, corresponding to times spaced by the period of Jupiter (about 12 years), while the behaviour of the comet outside this times is not captured by the stroboscopic map. As the transition is a quite fast phenomenon (it takes less than 2.5 years), this map will not show its details. In what follows we explain how we deal with these difficulties.

Let us start by selecting one torus (of the flow, hence, two-dimensional) around L_1 and one around L_2. We slice them with the temporal sections $\Sigma_{i\frac{\pi}{2}}$ defined by $f = i\frac{\pi}{2}$, $i = 0, 1, 2, 3$, where f is the true anomaly of the ERTBP (1). These are the temporal sections used in [DJ23a] to compute the invariant tori around $L_{1,2}$. Figure 8 shows (a projection of) these slices jointly with the position of Oterma in these sections. The initial data for Oterma has been selected when the comet is close to L_2 (see Section 2). For this initial data, as mentioned in Table 2, the value of the true anomaly is $f = 3.8817002439241626$. So, the positions plotted in Figure 8 were computed via forward integration for $\Sigma_{\frac{3\pi}{2}}$ and backward for the others.

Let us now choose one of the sections $\Sigma_{i\frac{\pi}{2}}$ to visualise the stable and unstable manifolds of the tori. We use (some of) the tori computed in [DJ23a]. We will use the same integer indices as in [DJ23a] to refer to them but we will add their frequencies to have a unique identification. So, we consider $T_j^{L_1}$ and $T_k^{L_2}$, where $j = -2565, \cdots, 4704$ and $k = -1330, \cdots, 2565$. The sets of indexes

Around L_1		Around L_2	
Name	ω (rotation number)	Name	ω (rotation number)
$T^{L_1}_{-2565}$	1.121174086130501	$T^{L_2}_{-1330}$	6.143937631678226
$T^{L_1}_{0}$	0.864674086131099	$T^{L_2}_{0}$	6.010937631678536
$T^{L_1}_{2000}$	0.664674086131565	$T^{L_2}_{2000}$	5.810937631679002
$T^{L_1}_{4704}$	0.394274086132195	$T^{L_2}_{3167}$	5.694237631679274

Table 3: Names of some special tori for used in this section. See [DJ23a] for details on how to name them.

are built as follows: the tori of indices $j = 0$ and $k = 0$ are the first computed ones (the ones coming from the periodic orbits related to the energy level $H = -1.5175$ in the PCRTBP), the tori with larger rotation number ω will be denoted by negative indexes (and they will be closer to L_j) and the ones with smaller rotation number will be assigned the positive indexes. Here we use the tori presented in Table 3. The reasons for the choice of these tori will be clearer later on.

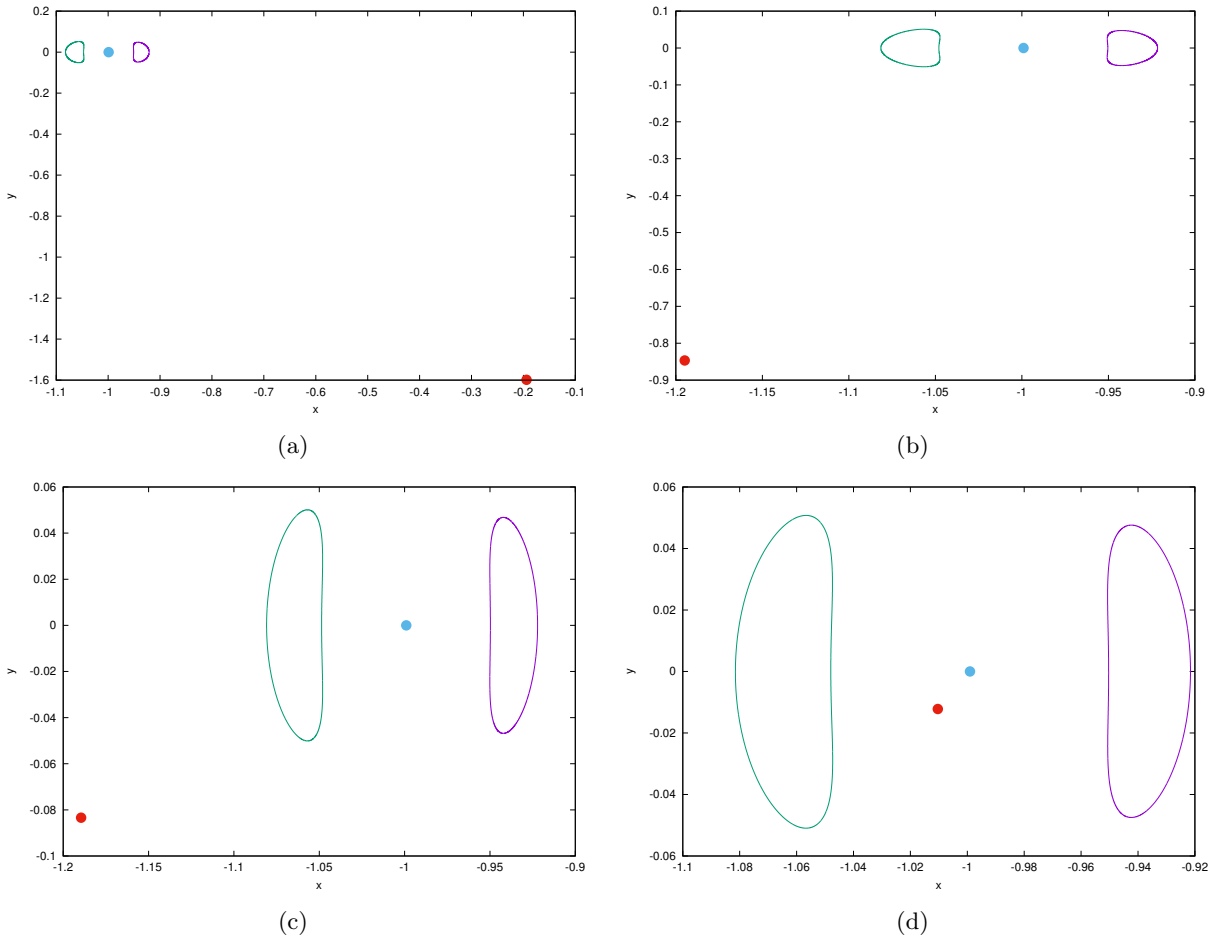

Figure 8: $T^{L_1}_{-2565}$ and $T^{L_2}_{-1330}$ together with Oterma, in red, and Jupiter, in blue, in (a) Σ_0, (b) $\Sigma_{\frac{\pi}{2}}$, (c) Σ_π, (d) $\Sigma_{3\frac{\pi}{2}}$.

Figure 8 shows the (x, y) projections of $T^{L_1}_{-2565}$ and $T^{L_2}_{-1330}$ for different temporal sections, mark-

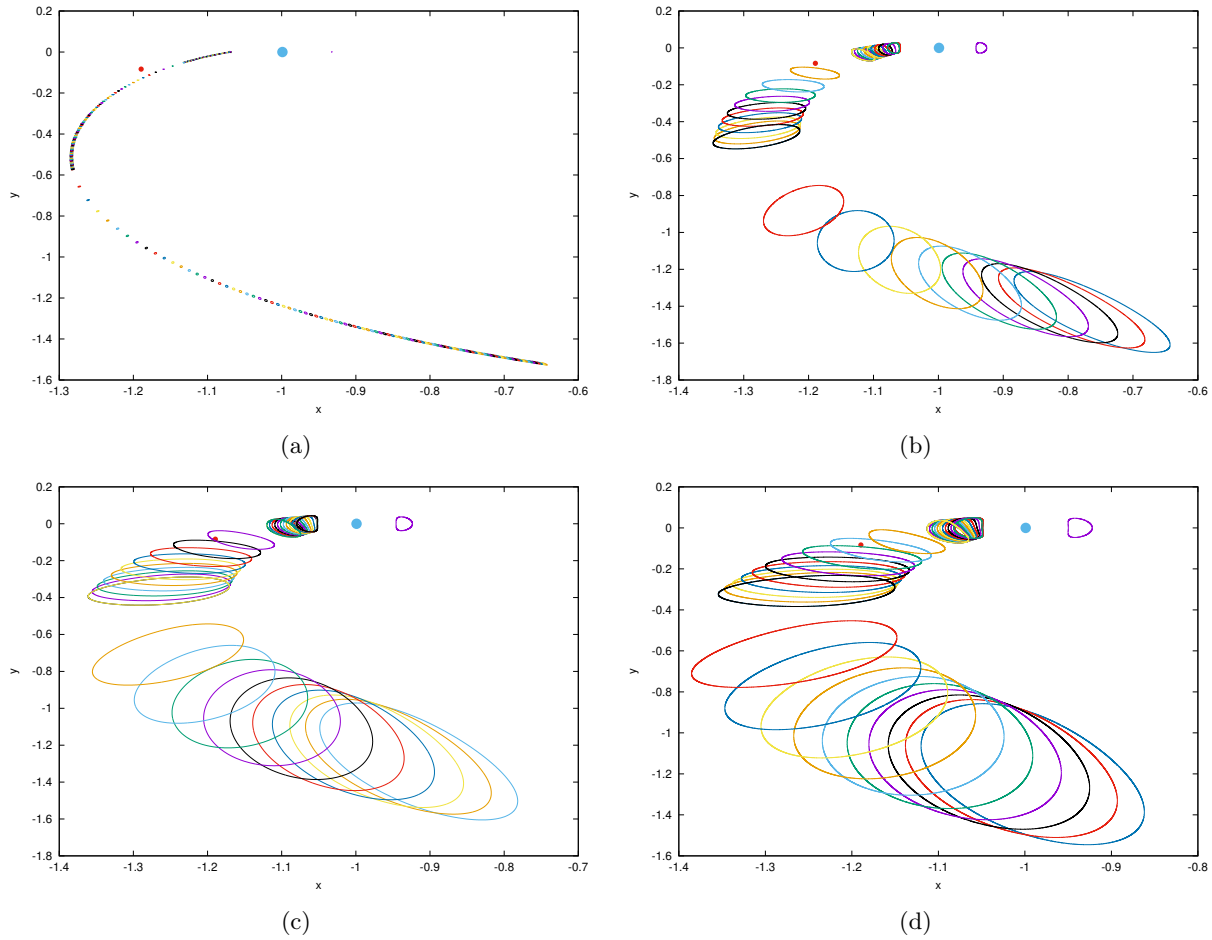

Figure 9: Plots of the stable manifolds of the tori (a) $T^{L_2}_{-1330}$, (b) $T^{L_2}_{0}$, (c) $T^{L_2}_{2000}$, (d) $T^{L_2}_{3167}$, together with Oterma position in section Σ_π. The red point is Oterma and the blue one Jupiter.

ing with a red dot the position of Oterma. Note that the time between these sections is 1/4 of the period of Jupiter, that is, nearly 3 years, which implies that the transition (that takes place in less than 2.5 years) could happen between two of these plots. Looking for a better section will not solve the problem since the transition cannot be visualised in a single stroboscopic section: Oterma is only a point in each of them, and in every section the invariant tori (and their manifolds) are different. On the other hand, from Table 2 we know that the transition is about to take place for $f \approx 3.88$ which means that the section Σ_π could be a good one to start the study.

Notice that Σ_π is a four-dimensional environment. It is not obvious how to visualise the manifolds and their influence on Oterma. For instance, Figure 9, that shows some slices of the stable manifold (seen as circular curves) of a tori around L_2 together with Oterma in the configuration space.

4.1 Slicing a stroboscopic map

It would be very useful to be able to perform a spatial slice of the phase space of the stroboscopic map, to reduce its dimension to 3. Although we cannot perform slices of orbits of discrete systems, we can slice invariant manifolds. In this way and invariant curve becomes a point (or a set of

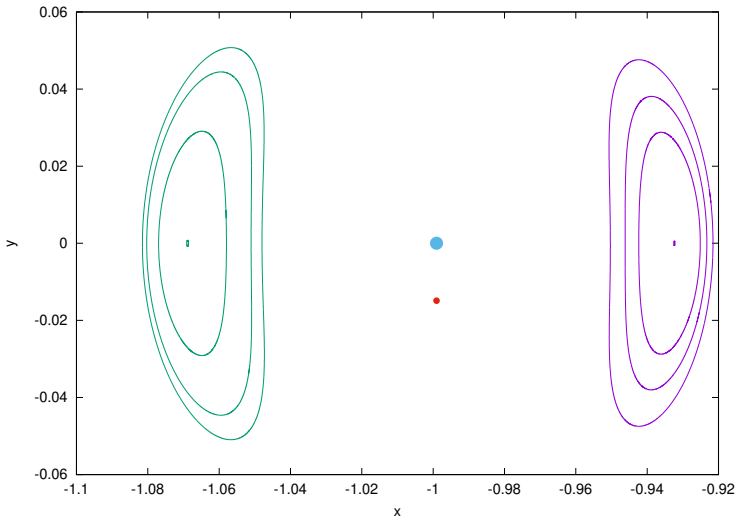

Figure 10: Some tori around L_1 and L_2 together with Oterma (red) and Jupiter (blue) in Σ_{f^*}. These tori are the ones whose manifolds were computed and will be shown in the following figures.

points), and its stable and unstable manifolds become curves. We note that these objects are not invariant by the discrete dynamics of the map.

Assume, for instance, that we want to visualise the position of the invariant curves and manifolds when Oterma has the same x coordinate as Jupiter. To this end, we integrate Oterma in the PERTBP till its x coordinate is the one of Jupiter, $x = \mu - 1$, which happens when the true anomaly is $f^* = 4.750563615740$. Now, we can recompute everything for the section Σ_{f^*} or, as f^* is slightly larger than $3\frac{\pi}{2} \approx 4.71238898$, we can transport by the flow of the ODE the invariant tori and manifolds from $\Sigma_{3\frac{\pi}{2}}$ to Σ_{f^*}. The result is that we have Oterma and the manifolds in the same three-dimensional manifold $\{f = f^*, x = -1 + \mu\}$. Figure 10 shows the (x, y) projection of some invariant curves of the stroboscopic map on the 4D section $f = f^*$, so that Oterma (red dot) has the same x coordinate as Jupiter (blue dot). Figure 11 shows the intersection of the invariant manifolds with the three-dimensional manifold $\{f = f^*, x = -1 + \mu\}$, including the position of Oterma as a red dot. The (y, p_y) projection of this plot is shown in Figure 12, where the purple curve at the left side of the plot is the unstable manifold of $T^{L_2}_{3167}$ and the green curve at the left is the stable manifold of $T^{L_1}_{4704}$. The two curves at the right side of the plot are the stable manifold of $T^{L_2}_{3167}$ (purple) and the unstable manifold of $T^{L_1}_{4704}$ (green).

Although the unstable manifold of $T^{L_2}_{3167}$ seems to intersect the stable manifold of $T^{L_1}_{4704}$, they simply come very close. If we move the value of f^* these two one-dimensional curves also move in $\mathbb{R}^3$ and, under generic transversality conditions, they will intersect for some value $\hat{f}$. This intersection gives an heteroclinic connection between these two tori.

As stated before, the codimension of the invariant manifolds of the invariant curves in a 4D stroboscopic section Σ_f is 2 and, therefore, they do not separate the phase space in different regions, i.e., there is not an "inside" and "outside" w.r.t. these manifolds. If these manifolds were of codimension 1 they would act as separatrices, in the sense that they would separate the trajectories that, for instance, approximates $T^{L_1}_{4704}$ and go inside towards $T^{L_2}_{3167}$ from the trajectories that approximates $T^{L_1}_{4704}$ and "bounce back" to the region outside the orbit of Jupiter. If, instead of the Planar ERTBP we were dealing with the Planar RTBP the situation would be completely different: the phase space is 4D, but fixing the energy level h and using a spatial section we obtain

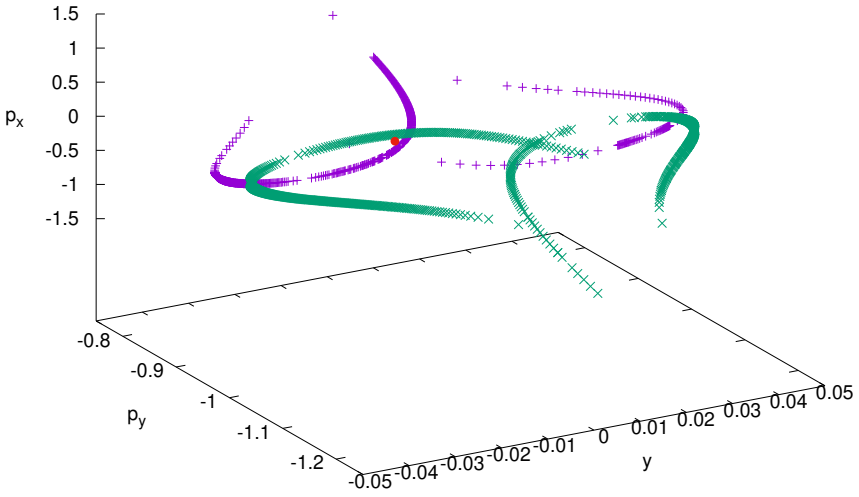

Figure 11: Invariant manifolds of the tori $T^{L_1}_{4704}$ (in green) and $T^{L_2}_{3167}$ (in purple) together with Oterma (red point).

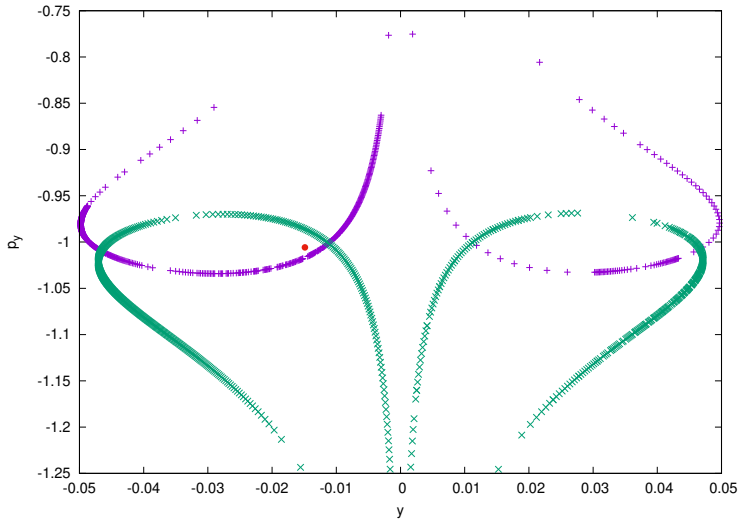

Figure 12: Projection on the (y, p_y) plane of Figure 11. See the text for more details.

a 2D map, where the invariant manifolds of the Lyapunov periodic orbits of $L_{1,2}$ are 1D so they separate the phase space. In the Sun-Jupiter Planar ERTBP, as the eccentricity of Jupiter is small, we are close to the Planar RTBP and this is seen, for instance, in the fact that the curves in Figure 11 are nearly coplanar. Therefore, although the curves of the manifolds do not separate phase space, we still observe that the "inner" and the "outer" regions shown in Figure 12 mostly have this behaviour: as example, Oterma (the red dot) is "inside" the green and purple curves so that it transits following these manifolds from outside the orbit of Jupiter to inside.

The intersections presented here are the first intersections of the manifolds with the sections, i.e., as it could be seen in [DJ23a], if we integrate for a longer time, the manifolds (or part of them) go away and come back will have more intersections, but, as we are interested in the Rapid Transition Mechanism, we discard the intersections of the manifolds after they revolve around Jupiter.

In [DJ23b], the frequencies of periodic orbits around L_1 and L_2 that adjust well to Oterma's orbit are computed. The ones with a better adjustment have the frequencies 2.06459523079767 and 1.90482664398271, respectively. For this work, we have that one of the frequencies of the computed tori is 1 (the frequency of the time dependence in the model) and the other one varies inside the intervals [2.06275066974076,2.17844039787426] (for the ones around L_1) and [1.90626606622183,1.97783804413025] (for the ones around L_2). We recall that the smaller the frequency the further the torus is from the equilibrium point. As $T^{L_1}_{4704}$ and $T^{L_2}_{3167}$ are the tori with greater frequency (2.06275066974076 and 1.90626606622183, respectively), we can see that they are near the ones that are born from these computed periodic orbits in the PCRTBP.

In summary, in this section we have seen that it is possible to identify the dynamical objects that guide Oterma in its transition between different regions in the configuration space of the PERTBP and visualize them together with Oterma using some temporal+spatial section that are ought to be chosen carefully. This is possible due to the usage of numerical techniques described in [Jor01, DJ23a], namely, how to compute a torus, how to continue it with respect to a parameter, how to compute its invariant stable and unstable manifolds and the usage of parallel shooting to diminish the instability involved in these computations; the possibility to fit Oterma in the PERTBP via a change of variables discussed in Section 3; and the fact that the PERTBP can be seen as a periodic perturbation of the PCRTBP where the theory of this transition mechanism is stated.

5 Conclusions and future work

In this paper we have used the invariant tori around the equilibrium points L_1 and L_2 of the Planar ETRBP and their stable/unstable manifolds (that were already computed in [DJ23a]) to study the transition of Oterma in this model.

To this end, we have translated the initial data of Oterma to the synodic coordinates of the ERTBP, and we have discussed the effect of choosing the initial conditions for the comet at different times. The numerical simulations show that the ERTBP is a much better model than the Circular RTBP used in previous studies. We have also shown how the stable and unstable manifolds of suitable tori guide Oterma in its fast transition from a region outside the orbit of Jupiter to a region inside.

It would be very interesting to consider the families of Lyapunov tori around $L_{1,2}$ as a single invariant manifold. This manifold has Cantorian structure but the holes due to the resonances are so small [JV97a, JV97b] that, for practical reasons, the manifold would be of dimension 2 for the

4D stroboscopic map. This manifold would have stable and unstable manifolds, each of dimension 3 and, therefore, they would separate the phase space and would act as barriers for the dynamics. However, their computation is much more demanding so this is left for a future work.

Another point worth considering would be to improve the model by adding the effect of Saturn.

5.1 The effect of Saturn

The addition of the effect of Saturn in this dynamics leads to a more accurate model. It extends the transition to times in which it does not happen when considering just the effects of the Sun and Jupiter. In Figure 4(a), we see that the numerical integration starting at November 1$^{\text{st}}$, 1980 (in the model Sun-Jupiter-Oterma) does not present the second transition, but adding the effect of Saturn, it does (as it may be seen in Figure 13(c)). In fact, it is even possible to extend more (Figure 13(b)), but this extension is limited (Figure 13(a)). An analogous argumentation might bo done for the comparison between Figures 4(d) and 13(d), together with the extension (Figures 13(e) and 13(f)).

In Figure 13(f) it is not possible to compute the semi-major axis of Oterma, because it does not return to the region between Jupiter and Saturn; instead it starts orbiting Jupiter as it can be seen in Figure 14.

In conclusion, we can see that the transition exists when considering only Sun, Jupiter and Oterma, with the drawback of restricting the time span of the integration.

References

[AEL17] R.L. Anderson, R.W. Easton, and M.W. Lo. Isolating blocks as computational tools in the circular restricted three-body problem. *Phys. D*, 343:38–50, 2017.

[DJ23a] G. Duarte and À. Jorba. Invariant manifolds near L_1 and L_2 in the Sun-Jupiter Elliptic Restricted Three-Body Problem I. Preprint, 2023.

[DJ23b] G. Duarte and À. Jorba. Using normal forms to study Oterma's transition in the planar RTBP. *Discrete Contin. Dyn. Syst. Ser. B*, 28:230–244, 2023.

[GL18] M. Guzzo and E. Lega. Geometric chaos indicators and computations of the spherical hypertube manifolds of the spatial circular restricted three-body problem. *Physica D: Nonlinear Phenomena*, 373:38–58, 2018.

[GLMS01] G. Gómez, J. Llibre, R. Martínez, and C. Simó. *Dynamics and mission design near libration points. Vol. I, Fundamentals: the case of collinear libration points*, volume 2 of *World Scientific Monograph Series in Mathematics*. World Scientific Publishing Co. Inc., 2001.

[JN20] À. Jorba and B. Nicolás. Transport and invariant manifolds near L_3 in the Earth-Moon bicircular model. *Commun. Nonlinear Sci. Numer. Simul.*, 89:105327, 2020.

[Jor01] À. Jorba. Numerical computation of the normal behaviour of invariant curves of n-dimensional maps. *Nonlinearity*, 14(5):943–976, 2001.

[JV97a] À. Jorba and J. Villanueva. On the normal behaviour of partially elliptic lower dimensional tori of Hamiltonian systems. *Nonlinearity*, 10:783–822, 1997.

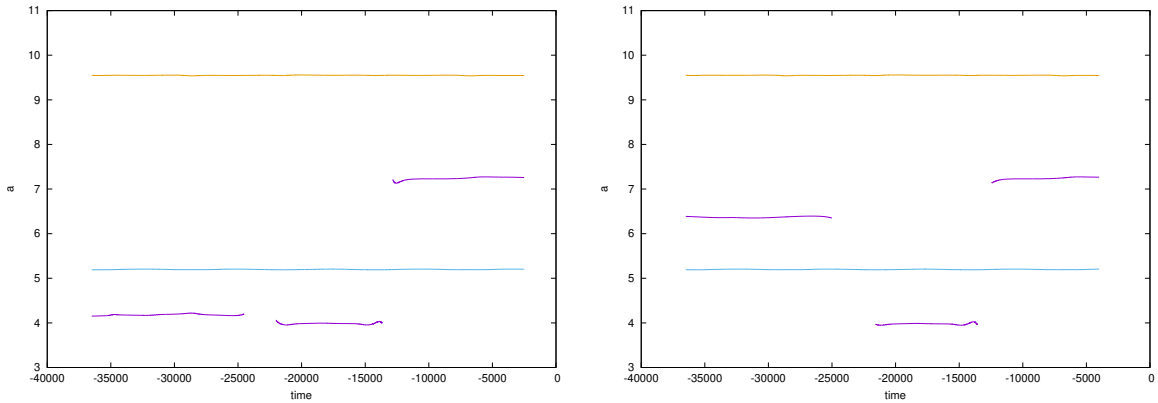

(a)

(b)

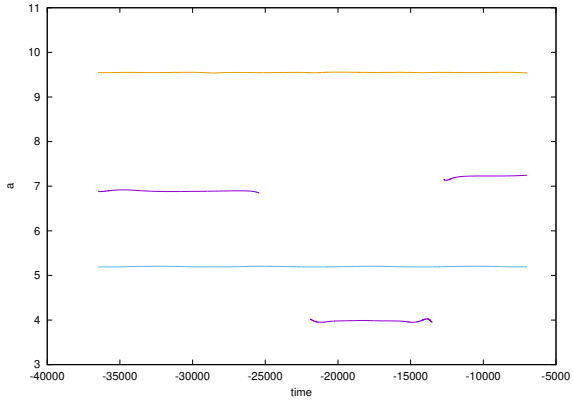

(c)

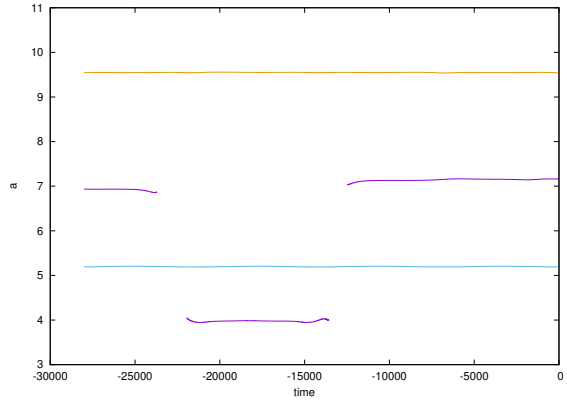

(d)

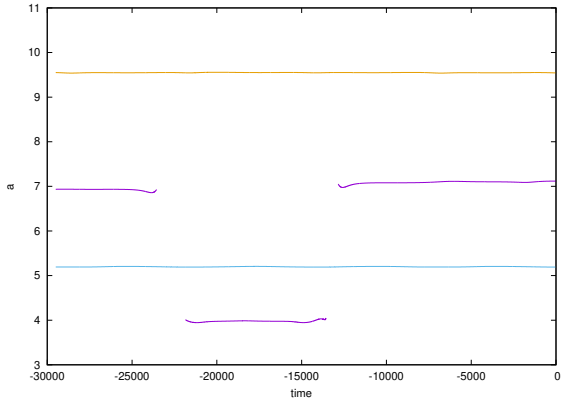

(e)

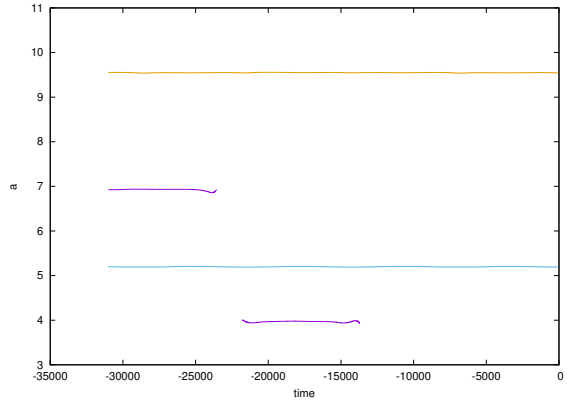

(f)

Figure 13: Computed semi-major axis of Jupiter, Saturn and Oterma. Units in AU and days. (a) Backward integration starting at $t = -2500$ (February 26$^{\text{th}}$, 1993); (b) Backward integration starting at $t = -4000$ (January 18$^{\text{th}}$, 1989); (c) Backward integration starting at $t = -7000$ (November 1$^{\text{st}}$, 1980); (d) Forward integration starting at $t = -28000$ (May 5$^{\text{th}}$, 1923); (e) Forward integration starting at $t = -29500$ (March 27$^{\text{th}}$, 1919); (f) Forward integration starting at $t = -31000$ (February 16$^{\text{th}}$, 1915). Time is given in days and distance in AU.

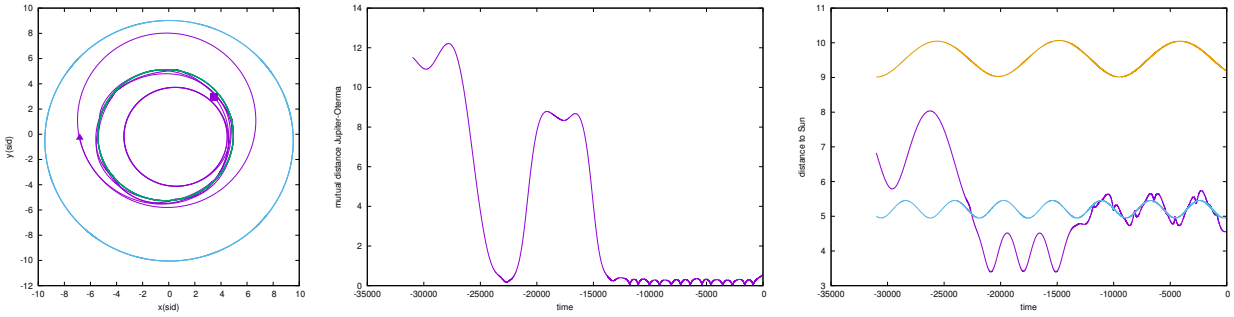

(a) (b) (c)

Figure 14: (a) Computed orbits of Jupiter, Saturn and Oterma, (b) mutual distance Jupiter-Oterma, and (c) distances Sun-Oterma, Sun-Jupiter and Sun-Saturn, all of them with initial data gathered in $t = -31000$ (February 16^{th}, 1915). Time is given in days and distance in AU.

[JV97b] À. Jorba and J. Villanueva. On the persistence of lower dimensional invariant tori under quasi-periodic perturbations. *J. Nonlinear Sci.*, 7:427–473, 1997.

[JZ05] À. Jorba and M. Zou. A software package for the numerical integration of ODEs by means of high-order Taylor methods. *Exp. Math.*, 14(1):99–117, 2005.

[KLMR01] W.S. Koon, M.W. Lo, J.E. Marsden, and S.D. Ross. Resonance and capture of Jupiter comets. *Celest. Mech. Dyn. Astron.*, 81(1-2):27–38, 2001.

[MO17] K.R. Meyer and D. Offin. *Introduction to Hamiltonian dynamical systems and the N-body problem*, volume 90 of *Applied Mathematical Sciences*. Springer, New York, third edition, 2017.

[OIY+08] K. Ohtsuka, T. Ito, M. Yoshikawa, D.J. Asher, and H. Arakida. Quasi-Hilda comet 147P/Kushida-Muramatsu - Another long temporary satellite capture by Jupiter. *Astron. Astrophys.*, 489(3):1355–1362, 2008.

[Pol66] H. Pollard. *Mathematical introduction to celestial mechanics*. Prentice-Hall, Inc., Englewood Cliffs, N.J., 1966.

[Roy04] A.E. Roy. *Orbital motion*. CRC Press, fourth edition, 2004.

[Sze67] V. Szebehely. *Theory of Orbits*. Academic Press, 1967.

[VM01] D.A. Vallado and W.D. McClain. *Fundamentals of Astrodynamics and Applications*. Fundamentals of Astrodynamics and Applications. Microcosm Press, 2001.